Solid State Phenomena Vol. 200 (2013) pp 73-78
© (2013) Trans Tech Publications, Switzerland
doi:10.4028/www.scientific.net/SSP.200.73

Crystallization Paths and Microstructure Formation in Ternary Oxide Systems with Stoichiometric Compounds

Vasily Lutsyk[a], Anna Zelenaya

Institute of Physical Materials Science (Siberian Branch of Russian Academy of Science),
6 Sakhyanova st., Ulan-Ude, 670047, Russian Federation

[a]vluts@ipms.bscnet.ru

Keywords: Space model, $CaO-SiO_2-Al_2O_3$ system, crystallization path, phases assemblage, microconstituent, mass balances.

Abstract. The problems of computer model engineering for a phase diagram of $CaO-SiO_2-Al_2O_3$ system are considered. The crystallization path and the formation of microconstituents in phases assemblage are analyzed for the surfaces of CaO, $3CaO\cdot SiO_2$ and $3CaO\cdot Al_2O_3$ primary crystallization. Two-dimensional, one-dimensional and zero-dimensional concentration fields were formed by the surfaces projection on the Gibbs triangle. Some one-dimensional and zero-dimensional concentration fields have no individuality and their microconstituents are the same as within the neighbor zero-dimensional and two-dimensional fields. The crystallization stages for given compositions are illustrated by the vertical and horizontal mass balances.

Introduction

Computer models of phase diagram is mounted of its phase regions with the designation of surfaces: liquidus ones, ruled surfaces, horizontal planes of solidus and the vertical triangulation planes. 3D model of this type permits to analyze the crystallization stages for any composition and to differ the concentration fields with individual set of microconstituents of phases assemblage and the concentration fields with the same crystallization schemes and microconstituents of phases assemblage as within the adjoining field.

Let's consider the system $CaO-SiO_2-Al_2O_3$, that has a great practical importance. The coordinates of binary and ternary invariant points are given as an initial data for the computer model of its phase diagram, simulated by means of kinematic surfaces [1]. Simulation of 3D model was complicated by the absence of unambiguous data both for the bounding binary systems and for the liquidus of ternary system.

Analysis of Literature Data

$CaO-Al_2O_3$. Many contradictions take place at the discussing of this system. The phase diagram of [2] has 5 compounds (2 incongruently melting phases C_3A, CA_6 and 3 ones $C_{12}A_7$, CA, CA_2 with congruent melting) (Fig. 1). In [3] a compound $C_{12}A_7$ is considered as a hydrate $Ca_{12}Al_{14}O_{32}(OH)_2$, that can't be found in system $CaO-Al_2O_3$, and a phase diagram has 4 compounds with incongruent melting (as was mentioned, the compound $C_{12}A_7$ was ignored), 4 peritectic points and one eutectic point. This variant of T-x-y diagram is confirmed by thermodynamic calculation [4] and by additional experimental investigation [5]. In [6, P. 34-38] it is stated that the existence of many variants of phase equilibrium in $CaO-Al_2O_3$ system depends on humidity and oxygen presence in the furnace atmosphere, which influence the composition of phase "$C_{12}A_7$". In this paper a binary phase diagram was used with 4 peritectic points, 2 eutectic points, 5 compounds (4 compounds C_3A, CA, CA_2, CA_6 with incongruent melting and a congruently melting compound $C_{12}A_7$). By the way, the phase $C_{12}A_7$ (or $C_{12}A_7H$) has been found as a natural mineral mayenite [7], and it has practical importance to produce dense ceramics [8].

Differences exist in thermodynamically calculated phase diagrams of this system too: calculated by Thermo-Calc diagram [9] coincides with data [3], but a diagram produced by the Fact Sage [10] includes 2 peritectic points, 3 eutectic points and 4 compounds (incongruently melting C_3A, CA_6 and congruently melting CA, CA_2).

In a diagram, obtained by the Calphad method, there are 4 peritectic points, 2 eutectic ones and 5 compounds (C_3A, CA_6, CA, CA_2 of incongruent melting and $C_{12}A_7$ of congruent melting) [11]. The authors explained that their previous calculation of this diagram didn't include the compound $C_{12}A_7$, since it's not strictly anhydrous [9]. But the cement phase diagrams contain the compound $C_{12}A_7$ as an aluminate phase [6, 12].

CaO-SiO_2. Experimental research CaO-SiO_2 [2, 6] revealed the immiscibility of two liquids and the associated points m & n on the monotectic segment, 3 peritectic points, 3 eutectic points, 4 compounds (congruently melting CS, C_2S and incongruently melting C_3S_2, C_3S). Other results of thermodynamic calculation also produced a similar variant of phase diagram [4, 11].

Calculated by Fact Sage diagram differs [13]. It includes the liquids immiscibility, only one peritectic point, 3 eutectic points and 4 compounds: CS and C_2S with congruent melting, C_3S_2 and C_3S with the decomposition below the liquidus curves. Besides a compound C_3S has low temperature of its stability too.

Al_2O_3-SiO_2. In most cases, the thermodynamically calculated diagrams of Al_2O_3-SiO_2 system [11, 14] correspond to the experimental data [2, 15]. Phase diagram contains two eutectic points as well as congruently melting compound A_3S_2.

CaO-SiO_2-Al_2O_3. Different interpretation of binary system CaO–Al_2O_3 produces different variants for a ternary phase diagram. Russian reference book [16] gives the CaO-SiO_2-Al_2O_3 T-x-y diagram as in [2]. Other variant of phase diagram [17] contains two additional surfaces of primary crystallization, corresponding to the same low temperature modification of compound C_2S. At that the CA_6 primary crystallization field is reduced and the coordinates of invariant quasiperitectic point Q_7 of reaction L+A=anortite+CA_6 (Fig. 1) differ from that suggested in [2, 16]. Besides the compound C_5A_3 was taken instead of $C_{12}A_7$. Similar phase diagram is reproduced in [14].

Other researchers [6, 12] present similar structure of liquidus, but without the additional primary crystallization fields corresponding to the C_2S low-temperature allotropy and denote the compound $C_{12}A_7$ instead of C_5A_3. And the structure of binary system CaO-Al_2O_3 differs from [2,17].

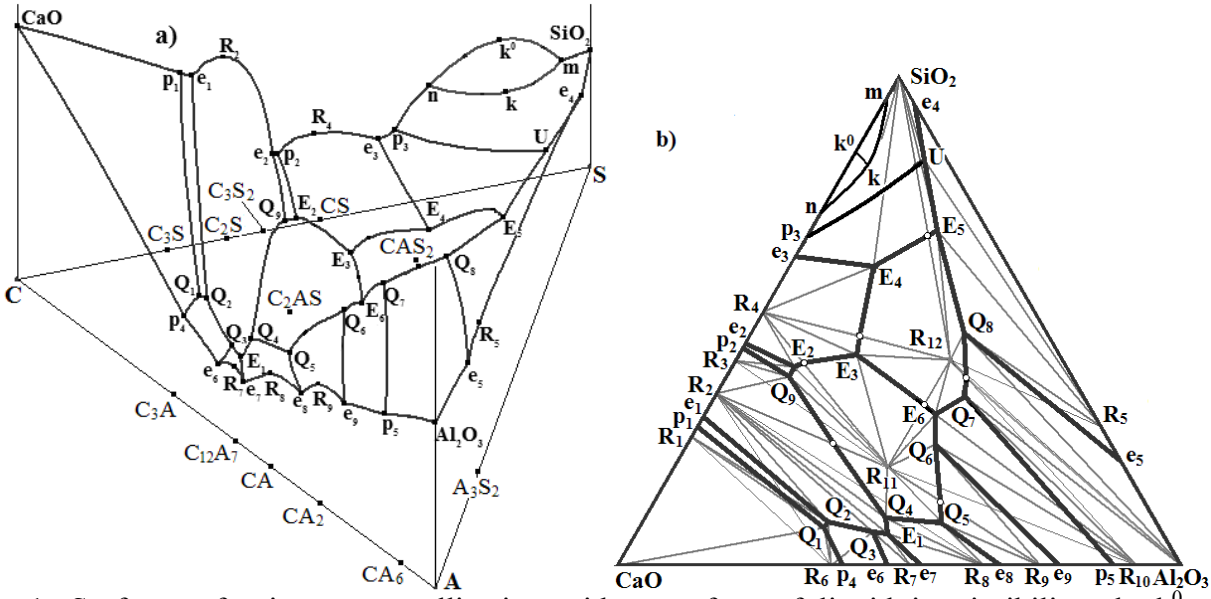

Fig. 1. Surfaces of primary crystallization with a surface of liquid immiscibility nkmk^0 and projection of all surfaces of (CaO-Al_2O_3-SiO_2)=(C-A-S) system (U – liquid phase, that participates in 4-phase reaction with 2 allotropies of SiO_2; E_1-E_6 & Q_1-Q_9 – ternary points of eutectics and quasiperitectics; R_1=C_3S, R_2=C_2S, R_3=C_3S_2, R_4=CS, R_5=A_3S_2, R_6=C_3A, R_7=$C_{12}A_7$, R_8=CA, R_9=CA_2, R_{10}=CA_6, R_{11}=C_2AS, R_{12}=CAS_2)

The thermodynamic calculation of ternary phase diagrams for the system CaO–SiO_2–Al_2O_3 have even more differences. Liquidus surfaces for compounds $C_{12}A_7$, A_3S_2 and $C_{12}A_7$ are absent in the diagram in [4], but an allotropy of compound C_2S has the additional primary crystallization surface. In model by V. Danek [18, P. 147] the immiscibility surface and 4 primary crystallization surfaces for compounds C_3S, C_3S_2, C_3A, CA_6 are absent. Three primary crystallization surfaces for the compounds C_3S, C_3S_2, $C_{12}Al_7$ are absent in the diagram calculated by CaTCalc [19].

Computer Model of System $CaO-Al_2O_3-SiO_2$

The experimental data [2] are used for computer model mounting. 14 binary points (9 eutectic (e) and 5 peritectic (p)), 16 ternary points (6 eutectic (E), 9 quasiperitectic (Q) and a point (U) of four-phase reaction $L_U+SiO_2^{cr} \leftrightarrows R_5+SiO_2^{tr}$ with two allotropies of SiO_2 (cr – crystobalite, tr – tridymite), 7 maximum points of the liquidus curves, 10 binary (R_1-R_{10}) and 2 ternary (R_{11}-R_{12}) compounds were taken as initial data. Phase diagram includes a cupola of liquid immiscibility, 16 surfaces of primary crystallization (Fig. 1), 80 ruled surfaces, 16 horizontal planes at the temperatures of invariant points and 16 vertical triangulation planes (that divide the phase diagram for the 15 subsystems). Phase diagram contains 33 two-phase regions (17 – with melt and 16 – without it) and 46 three-phase regions (31 – with melt and 15 – without it). The following designation of compounds are used: $R_1(C_3S)$, $R_2(C_2S)$, $R_3(C_3S_2)$, $R_4(CS)$, $R_5(A_3S_2)$ $R_6(C_3A)$, $R_7(C_{12}A_7)$, $R_8(CA)$, R_9CA_2), $R_{10}(CA_6)$, $R_{11}(C_2AS)$, $R_{12}(CAS_2)$, where R_1, R_3, R_6, R_{10} are melting incongruently and R_2, R_4, R_5, R_7, R_8, R_9, R_{11}, R_{12} are the congruently melting compounds.

Concentration Fields and Crystallization Paths

When phase regions of $CaO–Al_2O_3–SiO_2$ system [1] were projected to C-S-A triangle (Fig.1, b), it has given 117 two-, 163 one- and 45 zero-dimensional concentration fields. Analysis of 52 concentration fields (Fig. 2, a), that belong to the primary crystallization of component C(CaO) and neighbor compounds C_3S and C_3A (19 two-, 21 one- and 12 zero-dimensional fields) reveals that there are 18 fields (12 one-dimensional and 6 zero-dimensional) without the unique set of microconstituents (Table 1). At that, only within 2 one- and 1 zero-dimensional fields the crystallization stages and the microconstituents completely coincide with the adjoining fields: (R_6–3)∈(R_6–3–4), (Q_2–3)∈(Q_2-Q_3–4–3), 3∈(3–4), where sign ∈ means that first field belongs to the second one. Other 13 fields (8 one-dimensional and 5 – zero-dimensional) differ from their neighbors by the crossing surfaces and phase regions, but coincide in phase reactions and the set of microconstituents for the phase assemblages: (p_4-4)∈(p_4-4-Q_3-e_6), (3-4)∈(Q_2-Q_3-4-3), (3-Q_1)∈(Q_1-Q_2-3), (2-5)∈(R_1-1-2-5), (R_6-2)∈(R_6-1-2), (5-6)∈(R_1-5-6-7), (6-8)∈(6-7-8), (8-9)∈(p_1-7-8-9-e_1), 2∈(1-2), 5∈(R_1-5), 6∈(6-7), 8∈(7-8), 9∈(e_1-9). Two one-dimensional fields (Q_2-9)∈(Q_2-8-9) and (Q_1-Q_2)∈(Q_1-Q_2-8-6) haven't the unique microconstituents, but differ the neighbor two-dimensional fields by the scheme of solidification. These fields belong to the liquidus curves and therefore the reaction of primary crystallization $L^1 \rightarrow R_1^1$ is absent.

Table 1. Character of concentration field without the unique set of microconstituents

Fields	Intersecting phase regions	Scheme of solidification*	Microconstituents of Phases Assemblage
R_6-3∈** R_6-3-4	L+CaO, L+CaO+R_6, L+R_6, L+R_2+R_6, R_2+R_6+R_7	$L^1 \rightarrow CaO^1$, $L^{p4}+CaO^1 \rightarrow R_6^{p4}$, $L^{1p} \rightarrow R_6^{1p}$, $L^{ep} \rightarrow R_2^{R6,ep}+R_6^{R2,ep}$ $L^{Q3}+R_6 \rightarrow R_2^{Q3}+R_7^{Q3}$	R_6^{p4}, R_6^{1p}, $R_2^{R6,ep}$, $R_6^{R2,ep}$, R_2^{Q3}, R_7^{Q3}
Q_2-3∈ Q_2-Q_3-4-3	L+R_6, L+R_2+R_6, R_2+R_6+R_7	$L^1 \rightarrow R_6^1$, $L^e \rightarrow R_2^{R6}+R_6^{R2}$ $L^{Q3}+R_6 \rightarrow R_2^{Q3}+R_7^{Q3}$	R_6^1, R_2^{R6}, R_6^{R2}, R_2^{Q3}, R_7^{Q3}
3∈3-4	L+R_6, L+R_2+R_6, R_2+R_6+R_7	$L^1 \rightarrow R_6^1$, $L^e \rightarrow R_2^{R6}+R_6^{R2}$ $L^{Q3}+R_6 \rightarrow R_2^{Q3}+R_7^{Q3}$	R_6^1, R_2^{R6}, R_6^{R2}, R_2^{Q3}, R_7^{Q3}
2-5∈ R_1-1-2-5	L+CaO, L+CaO+R_1, L+R_1+R_6, R_2+R_6	$L^1 \rightarrow CaO^1$, $L^{p1}+CaO^1 \rightarrow R_1^{p1}$, $L^{Q1}+CaO^1 \rightarrow R_1^{Q1}+R_6^{Q1}$ $L^{ep} \rightarrow R_1^{R6,ep}+R_6^{R1,ep}$ $L^{Q2}+R_1 \rightarrow R_2^{Q2}+R_6^{Q2}$	R_1^{p1}, R_1^{Q1}, R_6^{Q1}, $R_1^{R6,ep}$, $R_6^{R1,ep}$, R_2^{Q2}, R_6^{Q2}
R_6-2∈	L+CaO,	$L^1 \rightarrow CaO^1$,	

R_6-1-2	L+CaO+R_6, L+R_1+R_6, R_2+R_6	L^{p4}+CaO^1→R_6^{p4}, L^{Q1}+CaO^1→R_1^{Q1}+R_6^{Q1} L^{ep}→$R_1^{R6,ep}$+$R_6^{R1,ep}$ L^{Q2}+R_1→R_2^{Q2}+R_6^{Q2}	R_6^{p4}, R_1^{Q1}, R_6^{Q1}, $R_1^{R6,ep}$, $R_6^{R1,ep}$, R_2^{Q2}, R_6^{Q2}
5-6∈ R_1-5-6-7	L+CaO, L+CaO+R_1, L+R_1, L+R_1+R_6, R_2+R_6	L^1→CaO^1, L^{p1}+CaO^1→R_1^{p1}, L^{1p}→R_1^{1p}, L^{ep}→$R_1^{R6,ep}$+$R_6^{R1,ep}$ L^{Q2}+R_1→R_2^{Q2}+R_6^{Q2}	R_1^{p1}, R_1^{1p}, $R_1^{R6,ep}$, $R_6^{R1,ep}$, R_2^{Q2}, R_6^{Q2}
2∈1-2	L+CaO, L+R_1+R_6, R_2+R_6	L^1→CaO^1, L^{Q1}+CaO^1→R_1^{Q1}+R_6^{Q1} L^{ep}→$R_1^{R6,ep}$+$R_6^{R1,ep}$ L^{Q2}+R_1→R_2^{Q2}+R_6^{Q2}	R_1^{Q1}, R_6^{Q1}, $R_1^{R6,ep}$, $R_6^{R1,ep}$, R_2^{Q2}, R_6^{Q2}
5∈R_1-5	L+CaO, L+CaO+R_1, L+R_1+R_6, R_2+R_6	L^1→CaO^1, L^{p1}+CaO^1→R_1^{p1}, L^{Q1}+CaO^1→R_1^{Q1}+R_6^{Q1}, L^{ep}→$R_1^{R6,ep}$+$R_6^{R1,ep}$ L^{Q2}+R_1→R_2^{Q2}+R_6^{Q2}	R_1^{p1}, R_1^{Q1}, R_6^{Q1}, $R_1^{R6,ep}$, $R_6^{R1,ep}$, R_2^{Q2}, R_6^{Q2}
6∈6-7	L+R_1, L+R_1+R_6, R_2+R_6	L^1→R_1^1, L^e→R_1^{R6}+R_6^{R1} L^{Q2}+R_1→R_2^{Q2}+R_6^{Q2}	R_1^1, R_1^{R6}, R_6^{R1}, R_2^{Q2}, R_6^{Q2}
6-8∈ 6-7-8	L+R_1, L+R_1+R_6, R_2+R_6	L^1→R_1^1, L^{e1}→R_1^{R6}+R_6^{R1} L^{Q2}+R_1→R_2^{Q2}+R_6^{Q2}	R_1^1, R_1^{R6}, R_6^{R1}, R_2^{Q2}, R_6^{Q2},
8-9∈ p_1-7-8-9-e_1	L+R_1, L+R_1+R_2, R_2+R_6	L^1→R_1^1, L^{e1}→R_1^{R2}+R_2^{R1} L^{Q2}+R_1→R_2^{Q2}+R_6^{Q2}	R_1^1, R_1^{R2}, R_2^{R1}, R_2^{Q2}, R_6^{Q2}
8∈7-8	L+R_1, R_2+R_6	L^1→R_1^1, L^{Q2}+R_1→R_2^{Q2}+R_6^{Q2}	R_1^1, R_2^{Q2}, R_6^{Q2}
9∈e_1-9	L+R_1+R_2, R_2+R_6	L^{e1}→R_1^{R2}+R_2^{R1} L^{Q2}+R_1→R_2^{Q2}+R_6^{Q2}	R_1^{R2}, R_2^{R1}, R_2^{Q2}, R_6^{Q2}
p_4-4∈ p_4-4-Q_3-e_6	L+R_6, L+R_6+R_7, R_2+R_6+R_7	L^1→R_6^1, L^{e6}→R_6^{R7}+R_7^{R6} L^{Q3}+R_6→R_2^{Q3}+R_7^{Q3}	R_6^1, R_6^{R7}, R_7^{R6}, R_2^{Q3}, R_7^{Q3}
3-4∈ Q_2-Q_3-4-3	L+R_6, L+R_2+R_6, R_2+R_6+R_7	L^1→R_6^1, L^e→R_2^{R6}+R_6^{R2} L^{Q3}+R_6→R_2^{Q3}+R_7^{Q3}	R_6^1, R_2^{R6}, R_6^{R2}, R_2^{Q3}, R_7^{Q3}
3-Q_1∈ Q_1-Q_2-3	L+R_6, L+R_1+R_6, L+R_2+R_6, R_2+R_6+R_7	L^1→R_6^1, L^e→R_1^{R6}+R_6^{R1} L^{Q2}+R_1→R_2^{Q2}+R_6^{Q2} L^{ep}→$R_2^{R6,ep}$+$R_6^{R2,ep}$ L^{Q3}+R_6→R_2^{Q3}+R_7^{Q3}	R_6^1, R_6^{R1}, R_2^{Q2}, R_6^{Q2}, $R_2^{R6,ep}$, $R_6^{R2,ep}$, R_2^{Q3}, R_7^{Q3}
Q_2-9∈ Q_2-8-9	L+R_1+R_2, L+R_2+R_6, R_2+R_6+R_7	L^{e1}→R_1^{R2}+R_2^{R1} L^{Q2}+R_1→R_2^{Q2}+R_6^{Q2} L^{ep}→$R_2^{R6,ep}$+$R_6^{R2,ep}$ L^{Q3}+R_6→R_2^{Q3}+R_7^{Q3}	R_2^{R1}, R_2^{Q2}, R_6^{Q2}, $R_2^{R6,ep}$, $R_6^{R2,ep}$, R_2^{Q3}, R_7^{Q3}
Q_1-Q_2∈ Q_1-Q_2-8-6	L+R_1+R_6, L+R_2+R_6, R_2+R_6+R_7	L^e→R_1^{R6}+R_6^{R1} L^{Q2}+R_1→R_2^{Q2}+R_6^{Q2} L^{ep}→$R_2^{R6,ep}$+$R_6^{R2,ep}$ L^{Q3}+R_6→R_2^{Q3}+R_7^{Q3}	R_6^{R1}, R_2^{Q2}, R_6^{Q2}, $R_2^{R6,ep}$, $R_6^{R2,ep}$, R_2^{Q3}, R_7^{Q3}

* type of reaction: ^{1}primary; $^{p,\ e}$monovariant peritectic and eutectic; ^{Q}invariant quasiperitectic; ^{ep}eutectic postperitectical; ^{1p}primary postperitectical; ^{E}invariant eutectic crystallization.

** ∈ - sign of coinciding (the same features as for the neighbor field with the larger dimension.

Let's consider the solidification of melt G within the triangle $R_1R_2R_7$ (two-dimensional field R_1-7-p_1). A composition G intersects the phase regions L+CaO, L+CaO+R_1, L+R_1, L+R_1+R_2, R_1+R_2+R_6 and the plane at temperature of invariant point Q_2. The composition of melt changes along the extension of segment CaO-G to liquidus curve p_1Q_1 (crystallization path G-a in Fig. 2a), when a centre of masses G passes through the region L+CaO. Then it falls into the regions L+CaO+R_1 and L+R_1 and the melt moves along a curve p_1Q_1 (a-b) and a liquidus surface $p_1Q_1Q_2e_1$ (b-c) correspondingly. Later a centre of masses G appears within the region L+R_1+R_2 and a path of L coincides with the curve e_1Q_2 up to the point Q_2 (c-Q_2). Below a plane at temperature Q_2 the liquid L doesn't exist, and composition G gets to the region R_1+R_2+R_6.

The mass balance diagram (Fig. 2, b) helps to deduce the crystallization stages and to estimate the phase portions. As could be seen from the diagram of mass balance, the following phase reactions: $L^1 \leftrightarrows CaO^1$, $L^{p1}+CaO^1 \leftrightarrows R_1{}^{p1}$, $L^{1p} \leftrightarrows R_1{}^{1p}$, $L^{ep} \leftrightarrows R_1{}^{R2,ep}+R_2{}^{R1,ep}$, $L^{Q2}+R_1 \leftrightarrows R_2{}^{Q2}+R_6{}^{Q2}$ take place for any composition of this concentration field. Since solidification finishes on the simplex $R_1R_2R_7$, then the crystals CaO^1 (expended in peritectic reaction) are absent as the microconstituent.

So the considered concentration field R_1-7-p_1 is characterized by the microconstituents (crystals of different origin): $R_1{}^{p1}$, $R_1{}^{1p}$, $R_1{}^{R2,ep}$, $R_2{}^{R1,ep}$, $R_2{}^{Q2}$, $R_6{}^{Q2}$.

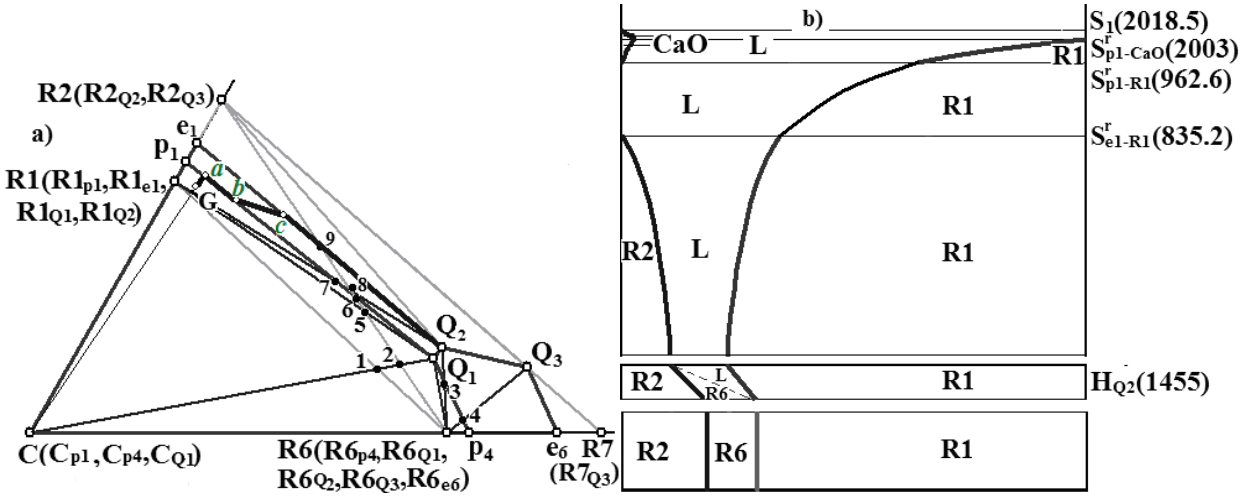

Fig. 2. Crystallization path G-1-2-3-Q_2 (a) and mass balances (b) in the process of melt solidification for composition G (compounds legends: R_1 – C_3S, R_2 –C_2S, R_6 –C_3A, R_7 – $C_{12}A_7$).

Summary

There are some variants of the CaO–Al_2O_3–SiO_2 phase diagram mainly due to differences in the structure of the CaO–Al_2O_3 binary system. In thermodynamic models of phase diagram the absence or distortion of the surfaces are associated with lack of thermodynamic data, and with the solving of practical tasks when some surfaces may be neglected. A suggested model of CaO–SiO_2–Al_2O_3 phase diagram will be useful as a template for other variants of the same diagram and for the oxide systems with similar topological features (MgO–Al_2O_3–SiO_2, Y_2O_3–Al_2O_3–SiO_2, FeO–Al_2O_3–SiO_2). It also permits to present a complete topological structure in order to highlight the phase regions and concentration fields with unique crystallization scheme.

References

[1] V.I. Lutsyk, A.E. Zelenaya, V.V. Savinov, Melt solidification in the ceramic system CaO-Al2O3-SiO2, IOP Conf. Ser.: Mater. Sci. Eng. 18 (2011) http://iopscience.iop.org/1757-899X/18/11/112005/pdf/1757-899X_18_11_112005.pdf.

[2] E.M. Levin, C.R. Robbins, H.F. McMurdie, Phase diagrams for ceramist, N.High.St, USA, Columbus, 1964.

[3] R.W. Nurse, J.H. Welch, A.J. Majumdar, The $CaO–Al_2O_3$ System in a Moisture-Free Atmosphere, Trans. Br. Ceram. Soc. 64 (1965) 409-418.

[4] R.G. Berman, T.H. Brown, A thermodynamic model for multicomponent melts, with application to the system $CaO-A1_2O_3-SiO_2$, Geochim. Cosmochim. Acta 48 (1984) 661-678.

[5] D.A. Jerebtsov, G.G. Mikhailov, Phase diagram of $CaO-Al_2O_3$ system, Ceram. Intern. 27 (2001) 25-28.

[6] H.F.W. Taylor, Cement Chemistry, Academic Press, London, 1990.

[7] G. Hentschel, Mayenit $12CaO·7Al_2O_3$ und Brownmillerit, $2CaO·(Al,Fe)·2O_3$, zwei neue Minerale in den Kalksteineinschlüssen der Lava des Ettringer Bellerberges, Neues Janrb. Mineral (1964) 22-29.

[8] A.S. Tolkacheva, S.N. Shkerin, S.V. Plaksin et al., Synthesis of dense ceramics of single-phase mayenite $(Ca_{12}Al_{14}O_{32})O$, Rus. J. App. Chem. 84 (2011) 907-911.

[9] H. Mao, M. Selleby, B. Sundman, A re-evaluation of the liquid phases in the $CaO–Al_2O_3$ and $MgO–Al_2O_3$ systems, Calphad 28 (2004) 307–312.

[10] Information on http://www.crct.polymtl.ca/fact/phase_diagram.php?file=Al-Ca-O_CaO-Al2O3.jpg&dir=FToxid.

[11] M.-N. de Noirfontaine, S. Tusseau-Nenez, C. Girod-Labianca, V. Pontikis, Calphad formalism for Portland clinker: Thermodynamic models and databases, J. Mat. Sci. 47 (2012) 1471-1479.

[12] F. Lea, Lea's Chemistry of Cement and Concrete, Elsevier Ltd, London, 1998.

[13] Information on http://www.crct.polymtl.ca/fact/phase_diagram.php?file=Ca-Si-O_CaO-SiO2.jpg&dir=FToxid.

[14] Information on http://www.crct.polymtl.ca/fact/phase_diagram.php?file=Al-Si-O_Al2O3-SiO2.jpg&dir=FToxid.

[15] A.A. Pashchenko, N.V. Aleksenko et al., Phisical Chemistry of Silicate, ed A.A. Pashchenko, Vyshcha schkola, Kiev, 1977 (In Russian).

[16] N.A. Toropov, V.P. Bazarkovsky, V.V. Lapshin et al., Diagram of Silicate System. Ternary Silicate Systems, vol 3, Nauka, Leningrad, 1972 (In Russian).

[17] A.L. Gentile, W.R. Foster, Calcium Hexaluminate and Its Stability Relations in the System $CaO-Al_2O_3-SiO_2$, J. Amer. Cer. Soc. 46 (1963) 74-76.

[18] V. Danek, Physico-chemical analysis of molten electrolytes, Elsevier, 2006.

[19] K. Shobu, CaTCalc: New thermodynamic equilibrium calculation software, Calphad 33 (2009) 279-287.